VI International Conference on Textile Composites and Inflatable Structures
STRUCTURAL MEMBRANES 2013
K.-U.Bletzinger, B. Kröplin and E. Oñate (Eds)

WIND-STRUCTURE INTERACTION SIMULATIONS FOR THE PREDICTION OF OVALLING VIBRATIONS IN SILO GROUPS

J. HILLEWAERE*, J. DEGROOTE†, G. LOMBAERT*, J. VIERENDEELS† AND G. DEGRANDE*

*Department of Civil Engineering, KU Leuven
Kasteelpark Arenberg 40, BE-3001 Heverlee, Belgium
e-mail: jeroen.hillewaere@bwk.kuleuven.be, web page: http://bwk.kuleuven.be/bwm

† Department of Flow, Heat and Combustion Mechanics, Ghent University
St. Pietersnieuwstraat 41, BE-9000 Gent, Belgium
web page: http://www.floheacom.ugent.be

Key words: Wind-structure interaction, CFD, silo, ovalling

Abstract. Wind-induced ovalling vibrations were observed during a storm in October 2002 on several empty silos of a closely spaced group consisting of 8 by 5 thin-walled silos in the port of Antwerp (Belgium). The purpose of the present research is to investigate if such ovalling vibrations can be predicted by means of numerical simulations. More specifically, the necessity of performing computationally demanding wind-structure interaction (WSI) simulations is assessed. For this purpose, both one-way and two-way coupled simulations are performed. Before considering the entire silo group, a single silo in crosswind is simulated. The simulation results are in reasonably good agreement with observations and WSI simulations seem to be required for a correct prediction of the observed ovalling vibrations.

1 INTRODUCTION

Wind-induced ovalling vibrations were observed during a storm in October 2002 on several empty silos of a closely spaced group consisting of 8 by 5 thin-walled silos in the port of Antwerp (Belgium) [4]. Wind-induced vibrations can be caused by either forced resonance or aeroelastic effects. In the first case, the forced vibrations originate from turbulent fluctuations in the wind flow around the structure, e.g. from natural turbulence in the wind flow attacking the structure or due to periodic vortex shedding in the wake of the structure. The second, aeroelastic phenomena are typically self-excited and are due to displacements of the structure and resulting interactions with the wind flow.

(a)  (b) 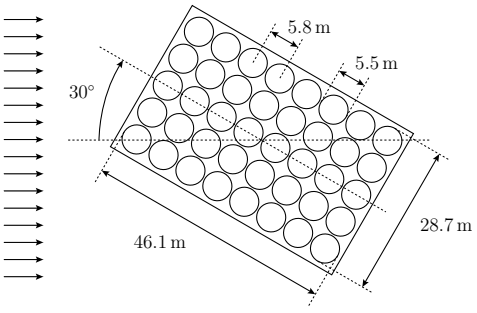

Figure 1: (a) Photo and (b) schematic representation of the 8 by 5 silo group in Antwerp (Belgium).

Flow-induced vibrations can be initiated by a combination of different phenomena and it is mostly impossible to pinpoint one specific excitation mechanism as the cause of an observed vibration [6]. The goal in this work is to investigate if advanced numerical techniques can adequately predict observed vibrations for such wind-structure interaction (WSI) problems. For this purpose, the coupled multiphysics problem considering both wind flow and structural dynamics has to be solved numerically.

The outline of this paper is as follows. First, the methodology for the numerical simulation of the WSI problem is considered (section 2). Both the structural and wind flow solvers are introduced but the emphasis is on the coupling approaches to investigate the influence of aeroelastic effects on the structural response. Afterwards, the coupling approaches are applied to the present application. First, the WSI problem of a single silo is simulated (section 3) and finally, the silo group is considered (section 4).

2 NUMERICAL METHODOLOGY FOR WSI SIMULATIONS

To solve the present WSI problem numerically, a partitioned approach is considered where the flow and structural equations are solved separately. The interaction between both domains is only enforced at the interface between the wind flow and the structure. In the following, first the structural and wind flow solvers are introduced (sections 2.1 and 2.2). To investigate if the observed ovalling vibrations are the result of forced resonance or aeroelastic effects, two different simulation approaches are explained afterwards (section 2.3) and a technique to compare the structural response in both approaches is given (section 2.4).

2.1 Structural model and ovalling modes of a silo

A numerical finite element (FE) model of the silo structure is constructed in the Abaqus software package [2] that allows to calculate the structural response of the silos to applied aerodynamic pressures. This model is also used to determine the ovalling eigenmodes and corresponding natural frequencies of the silos.

Ovalling deformations of a thin-walled shell structure are defined as a deformation of the cross section of the structure without bending deformation with respect to the

longitudinal axis of symmetry [7]. The ovalling mode shapes for the thin-walled empty silos (diameter 5.5 m and wall thickness varying from 0.07 m to 0.10 m along the height of the silo) are referred to by a couple (m, n) where m denotes the half wave number in the axial direction and n is the number of circumferential waves (figure 2).

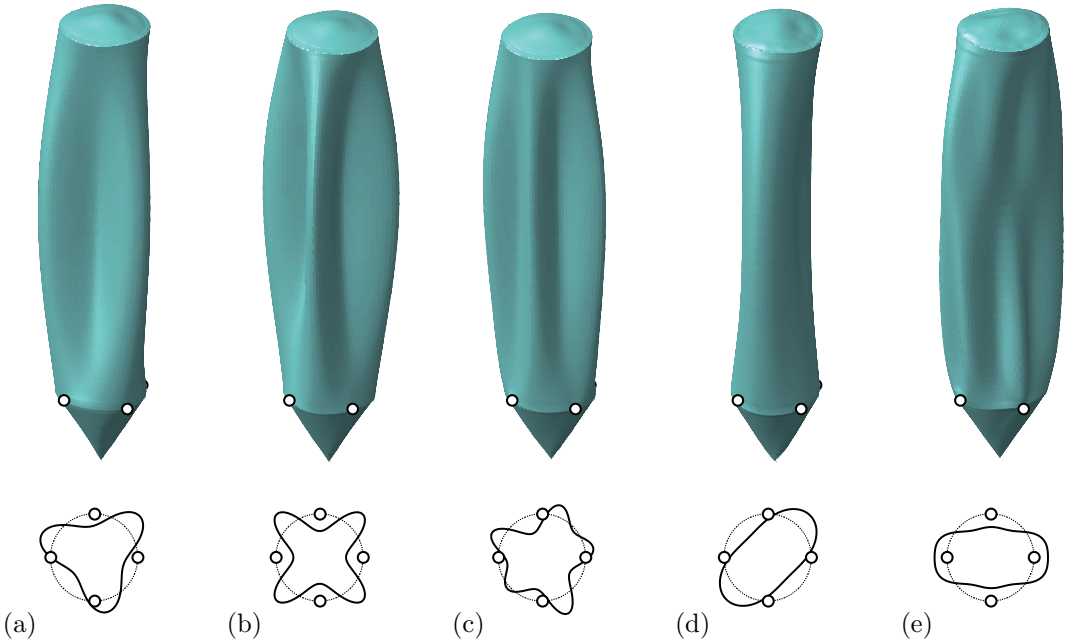

Figure 2: 3D isotropic view and horizontal section at mid-height for a selection of ovalling eigenmodes of a silo: (a) mode $\mathbf{\Phi}_1 = (1, 3)$ at 3.96 Hz, (b) mode $\mathbf{\Phi}_4 = (1, 4)$ at 4.11 Hz, (c) mode $\mathbf{\Phi}_5 = (1, 5)$ at 5.34 Hz, (d) mode $\mathbf{\Phi}_{11} = (1, 2)$ at 7.83 Hz and (e) mode $\mathbf{\Phi}_{14} = (2, 6)^*$ at 8.62 Hz.

To accommodate an easy transfer of the aerodynamic pressures on the silo walls to the mesh of the structural model in the coupled simulations (section 2.3), the mesh of the FE model is chosen conforming to the mesh on the silo walls in the wind flow simulations (section 2.2). Shell elements with linear FE interpolation functions are used for all silo elements and the following material properties for aluminium are used: density $\rho = 2700\,\mathrm{kg/m^3}$, Young's modulus $E = 67.6\,\mathrm{GPa}$ and Poisson's ratio $\nu = 0.35$. The silo structures are bolted to a steel framework in the supporting building at 4 discrete points.

A list of the mass normalized eigenmodes $\mathbf{\Phi}$ of the structure corresponding to the lowest natural frequencies f_{eig} is given in table 1. Note that most modes come in pairs: e.g. $\mathbf{\Phi}_1$ and $\mathbf{\Phi}_2$ are both classified as $(1, 3)$ but are mutually orthogonal.

The visually detected pattern of vibrations at the lee side of the silo group during the 2002 storm is believed to have been a combination of ovalling mode shapes $(1, 3)$ and $(1, 4)$, corresponding to the lowest eigenfrequencies. Measurements during normal wind loading have also shown that eigenmodes with 3 or 4 circumferential wavelengths have the highest contribution to the response of the silos [4].

Table 1: Structural natural frequencies f_{eig} of the lowest ovalling eigenmodes of the silo structure. Every mode $\mathbf{\Phi}_j$ is determined by a couple (m, n) while $\mathbf{\Phi}_{14}$ cannot be clearly classified as a single shape (m, n). The notation $(2, 6)^*$ is adopted because this mode could be classified as either shapes $(2, 6)$ or $(1, 2)$.

$\mathbf{\Phi}_j$	(m, n)	$f_{\text{eig}j}$ [Hz]	$\mathbf{\Phi}_j$	(m, n)	$f_{\text{eig}j}$ [Hz]	$\mathbf{\Phi}_j$	(m, n)	$f_{\text{eig}j}$ [Hz]
$\mathbf{\Phi}_1$	$(1, 3)$	3.96	$\mathbf{\Phi}_7$	$(1, 5)$	5.70	$\mathbf{\Phi}_{13}$	$(2, 5)$	8.19
$\mathbf{\Phi}_2$	$(1, 3)$	3.97	$\mathbf{\Phi}_8$	$(1, 5)$	5.71	$\mathbf{\Phi}_{14}$	$(2, 6)^*$	8.62
$\mathbf{\Phi}_3$	$(1, 4)$	3.99	$\mathbf{\Phi}_9$	$(1, 6)$	7.72	$\mathbf{\Phi}_{15}$	$(2, 4)$	8.85
$\mathbf{\Phi}_4$	$(1, 4)$	4.11	$\mathbf{\Phi}_{10}$	$(1, 6)$	7.72	$\mathbf{\Phi}_{16}$	$(2, 4)$	9.10
$\mathbf{\Phi}_5$	$(1, 5)$	5.34	$\mathbf{\Phi}_{11}$	$(1, 2)$	7.83	$\mathbf{\Phi}_{17}$	$(2, 6)$	9.62
$\mathbf{\Phi}_6$	$(1, 5)$	5.35	$\mathbf{\Phi}_{12}$	$(2, 5)$	8.18	$\mathbf{\Phi}_{18}$	$(2, 6)$	9.72

2.2 Wind flow simulations

To determine the aerodynamic pressures acting on the silo surfaces, the wind flow around the silo group is simulated in 3D computational fluid dynamics (CFD) simulations. The governing incompressible Navier-Stokes equations are discretized by means of the finite volume method in the commercial software package Fluent [1].

Because a high Reynolds number wind flow is considered, detached eddy simulations (DES) are used [9]. This hybrid RANS/LES method combines large eddy simulation (LES) in the far field where large turbulent structures are present with the RANS (Reynolds-averaged Navier-Stokes) approach in the near-wall regions. This is an interesting technique for highly turbulent flows, where it is in practice impossible to use LES simulations because of the prohibitive grid requirements to model the small turbulent eddies in near-wall flows. A delayed DES approach (DDES) is applied in which a shielding function is used to ensure that RANS is retained in the entire near-wall region which may lead to doubtable accuracy in separated regions [5].

Since exact atmospheric conditions near the silo group were not monitored at the time of the ovalling vibrations, approximate wind conditions have been set up, based on location and statistical wind data for storm conditions in design codes. The rectangular silo group is therefore rotated at an angle of 30° to the incident wind flow (figure 1b). For the atmospheric boundary layer (ABL), realistic power law velocity and turbulence profiles [10] are imposed at the inlet of the computational domain while for the generation of fluctuating velocity components, a spectral synthesizer method is used as proposed by [8].

In WSI problems, the interface between wind flow and solid deforms. To allow the deformation of a boundary in the fluid solver, the arbitrary Lagrangian-Eulerian (ALE) approach is used for the CFD simulation as incorporated in Fluent [1]. The displacement of the interface is extended into the entire fluid domain by adjusting the fluid grid accordingly which can be achieved by applying a spring smoothing or Laplacian smoothing method. Because of the lower computational cost, the spring smoothing method is preferred. However, when structural displacements are large, the Laplacian smoothing

method has to be used which leads to a drastic increase in simulation time. This is because the diffusion equation of the mesh velocities then has to be solved iteratively in every coupling iteration of the two-way coupled simulation.

2.3 WSI coupling approaches

From a computational point of view, it is important to assess the necessity of performing the computationally much more intensive WSI, two-way coupled simulations. Therefore, more straightforward one-way coupled simulations are performed as well. Performing both coupling approaches allows to investigate the importance of aeroelastic effects for the onset of ovalling vibrations and are discussed in more detail in the following.

A partitioned approach is followed in the simulations. This implies that the structural and flow solver remain separated, black box solvers and the interaction between both domains is incorporated only at the interface. In this framework, the structural FE solver (section 2.1) is denoted as $\boldsymbol{\mathcal{S}}[\mathbf{P}(t)] = \mathbf{U}(t)$, where $\mathbf{U}(t)$ are the displacements of the structure on the interface between fluid and structural solver and $\mathbf{P}(t)$ are the aerodynamic pressures acting on the structure. Similary, the CFD solver for the wind flow (section 2.2) is expressed as $\boldsymbol{\mathcal{F}}[\mathbf{U}(t)] = \mathbf{P}(t)$.

One-way coupled simulations

A one-way coupled simulation can be regarded as a special case of WSI simulation in which the structure is considered as a rigid body in the wind flow simulation. The time history of surface pressures on the rigid body structure is determined in the separate flow solver: $\boldsymbol{\mathcal{F}}[\mathbf{0}] = \mathbf{P}(t_i)$. As illustrated in figure 3, the resulting time history of aerodynamic surface pressures $\mathbf{P}(t)$ is subsequently applied as an external transient load on the structure and the structural response is computed in the structural solver for the entire time frame considered: $\boldsymbol{\mathcal{S}}[\mathbf{P}(t)] = \mathbf{U}(t)$.

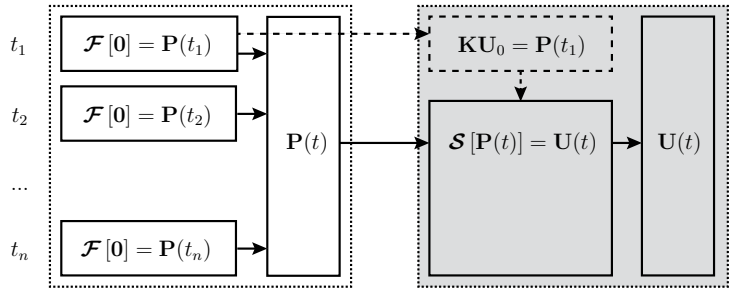

Figure 3: Schematic representation of the interaction between flow solver (white) and structural solver (grey) in the one-way partitioned coupling simulation.

To avoid a long transitional regime due to the abrupt application of the wind pressures on the undeformed silo structure, a static step preceding the dynamic calculation

is introduced: $\mathbf{K}\mathbf{U}_0 = \mathbf{P}_0$ with $\mathbf{K}$ the FE stiffness matrix of the structure. The applied pressures in this static step are taken equal to the pressures in the first dynamic time step: $\mathbf{P}_0 = \mathbf{P}(t_1)$. The effect of such preliminary static calculation where the structural response $\mathbf{U}_0$ is used as an initial condition for the dynamic calculations was found very effective.

Two-way coupled simulations

In two-way coupled simulations, the structural and flow solver are coupled in every time step as illustrated schematically in figure 4. As opposed to the one-way coupling approach, these simulations are WSI simulations in the true sense. An implicit (or strongly coupled) partitioned technique is used to ensure equilibrium at the interface in every time step. The IQN-ILS method is applied for this purpose in the present simulations [3].

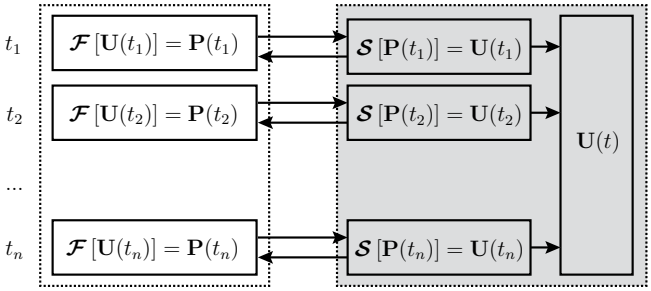

Figure 4: Schematic representation of the interaction between flow solver (white) and structural solver (grey) in the two-way partitioned coupling approach.

2.4 Modal deformation energy

For the physical interpration of the structural response in both one-way and two-way coupled simulations, the deformation energy per structural eigenmode is considered. The deformation energy $E_\mathrm{d}(t)$ of the structural response can be easily calculated from known displacements $\mathbf{U}(t)$:

$$E_\mathrm{d}(t) \quad = \tfrac{1}{2}\,\mathbf{U}^\mathrm{T}(t)\,\mathbf{K}\,\mathbf{U}(t), \tag{1}$$

where $\mathbf{K}$ is the FE stiffness matrix of the silo structure. In order to distinguish the contribution of the different eigenmodes in the response, modal decomposition is applied. By inserting $\mathbf{U}(t) = \boldsymbol{\Phi}\boldsymbol{\alpha}(t)$ in equation (1), the energy content of each eigenmode in the response can be quantified:

$$E_\mathrm{d}(t) \quad = \tfrac{1}{2}\,\boldsymbol{\alpha}^\mathrm{T}(t)\,\boldsymbol{\Phi}^\mathrm{T}\mathbf{K}\boldsymbol{\Phi}\,\boldsymbol{\alpha}(t) = \tfrac{1}{2}\,\sum_{j=1}^{n_\mathrm{DOF}} \omega_j^2 \alpha_j^2(t) = \sum_{j=1}^{n_\mathrm{DOF}} E_{\mathrm{d}j}(t). \tag{2}$$

These scalar energy expressions where n_{DOF} represents the total number of degrees of freedom in the FE model, allows to calculate the energy contribution $E_{\mathrm{d}j}(t)$ of every seperate mode j to the structural response using only the modal coordinates $\boldsymbol{\alpha}(t)$.

In the present one-way and two-way coupled simulations, the structural response $\mathbf{U}(t)$ is determined using direct time integration. The entire basis of n_{DOF} eigenmodes $\boldsymbol{\Phi}$ would therefore have to be determined to extract the modal coordinates $\boldsymbol{\alpha}(t)$. It is computationally very demanding, however, to solve the entire eigenvalue problem and only the lowest eigenmodes are relevant for a typical low frequency wind excitation. It is therefore desirable to use only a limited subset of $n_{\mathrm{s}} < n_{\mathrm{DOF}}$ eigenmodes $\boldsymbol{\Phi}_{\mathrm{s}}$ with corresponding modal coordinates $\boldsymbol{\alpha}_{\mathrm{s}}(t)$ to determine the deformation energy. It can be easily shown that these expressions hold when a pseudoinverse of $\boldsymbol{\Phi}_{\mathrm{s}}$ is introduced to determine the modal coordinates $\boldsymbol{\alpha}_{\mathrm{s}}(t)$ for this subset of mode shapes: $\boldsymbol{\alpha}_{\mathrm{s}}(t) = \boldsymbol{\Phi}_{\mathrm{s}}^{\mathrm{T}}\mathbf{M}\mathbf{U}(t)$.

3 SINGLE SILO SIMULATIONS

For the **one-way coupled single silo simulation**, the modal deformation energy components $E_{\mathrm{d}j}(t)$ of the structural response are shown as a function of time in figure 5 for the 20 lowest structural eigenmodes. Only a limited number of modes contribute significantly to the structural response of the silo but seemingly random fluctuations are observed in the stationary response. A distinction is therefore first made beween static and different fluctuating components in the response.

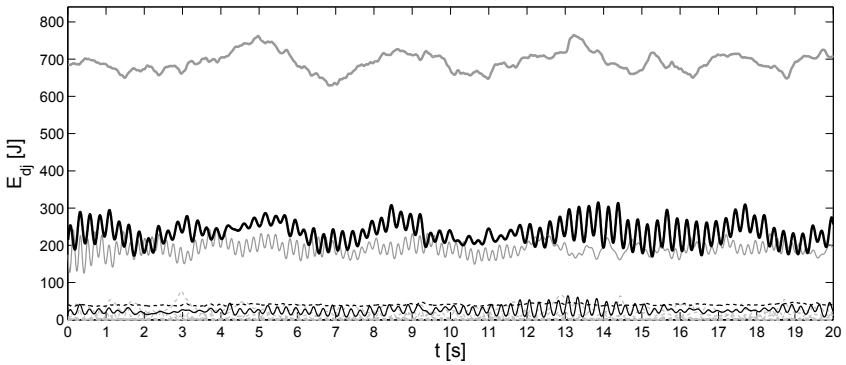

Figure 5: Modal deformation energy $E_{\mathrm{d}j}(t)$ for the first 20 mode shapes, based on the structural response in the one-way coupled simulation of a single silo: $\boldsymbol{\Phi}_2 = (1,3)$ (bold black line), $\boldsymbol{\Phi}_4 = (1,4)$ (thin black line), $\boldsymbol{\Phi}_6 = (1,5)$ (thin grey line), $\boldsymbol{\Phi}_{14} = (2,6)^*$ (bold grey line), $\boldsymbol{\Phi}_{18} = (2,6)$ (dashed black line), and the remaining mode shapes $\boldsymbol{\Phi}_j$ (dashed grey lines, with small energy content).

The mean, time averaged modal deformation energy is related to the static excitation of a structural eigenmode. This is e.g. the case for mode shape $\boldsymbol{\Phi}_{18} = (2,6)$ that is almost exclusively excited statically (dashed black line in figure 5). In the fluctuating parts of the response, a further distinction can be made between two components.

The first is related to large scale turbulent eddies present in the wind flow in vicinity of the silo structure. The fourteenth mode $\boldsymbol{\Phi}_{14} = (2,6)^*$ is e.g. mostly excited by such low

frequency fluctuations (bold grey line in figure 5). These oscillations are referred to as quasi-static or background vibrations because they are free of any resonant effects. While the exact origins of these low frequency fluctuations are not easily identified, it is possible that they originate from the turbulent fluctuations in the incident wind flow. Because the wind flow fluctuations are generated at the inlet of the computational domain including random numbers, these low frequency fluctuations are not exactly the same in different CFD simulations.

The second type of fluctuating components in the response are exactly at the eigenfrequencies of the eigenmodes and are hence related to forced resonance in the one-way coupled simulations.

Based on this description, an alternative way to represent the results is to consider the time averaged and RMS values of the modal deformation energy, $\overline{E}_{\mathrm{d}j}$ and $E_{\mathrm{d}j}^{\mathrm{RMS}}$. Figure 6 shows these quantities for the one-way coupled simulation of the single silo for the 50 lowest eigenmodes. The mean modal deformation energy $\overline{E}_{\mathrm{d}j}$ (figure 6a) gives an indication of the static excitation of the eigenmodes while the RMS values $E_{\mathrm{d}j}^{\mathrm{RMS}}$ contain information on all dynamic excitations, both quasi-static and resonant. These figures allow to qualitatively compare the response in different coupled simulations.

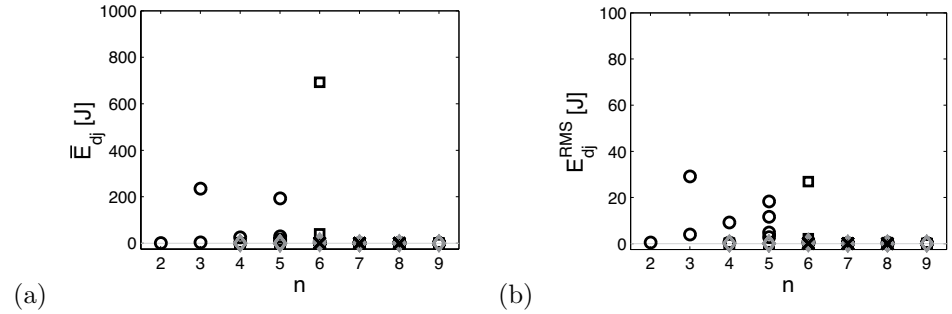

(a) (b)

Figure 6: (a) Mean and (b) RMS of modal deformation energy $E_{\mathrm{d}j}(t)$ of the structural response of the single silo in the one-way coupled simulation. The deformation energy for the lowest 50 eigenmodes is plotted as a function of n while separate mode shapes $(1, n)$ are depicted as a circle ($\circ$), $(2, n)$ as a square ($\square$), $(3, n)$ as a diamond ($\Diamond$), and $(4, n)$ as a cross ($\times$).

Based on the comparison of figures 6a and 6b, it is clear that structural vibrations will be much smaller than the static displacements. In general terms, the vibration amplitudes are in the order of 0.5 to 1 cm while the peak displacement is approximately 4 cm for this single silo. The eigenmodes that are mainly excited statically are $\mathbf{\Phi}_2 = (1, 3)$, $\mathbf{\Phi}_6 = (1, 5)$ and $\mathbf{\Phi}_{14} = (2, 6)^*$ while mainly the eigenmodes with the lowest circumferential wavenumber n and only a half wavelength accross the height ($m = 1$) are excited dynamically. The excitation of $\mathbf{\Phi}_{14} = (2, 6)^*$ is mainly quasi-static and related to the presence of a bolted connection at the windward side of the silo.

In the **two-way coupled simulation** of the single silo, spring smoothing is used for the ALE mesh motion in the CFD solver and in general 5 IQN-ILS coupling iterations

have to be performed in each time step to ensure equilibrium on the WSI interface. The computational effort for the two-way coupled simulations is therefore said to be approximately 5 times larger than for the one-way coupled simulations.

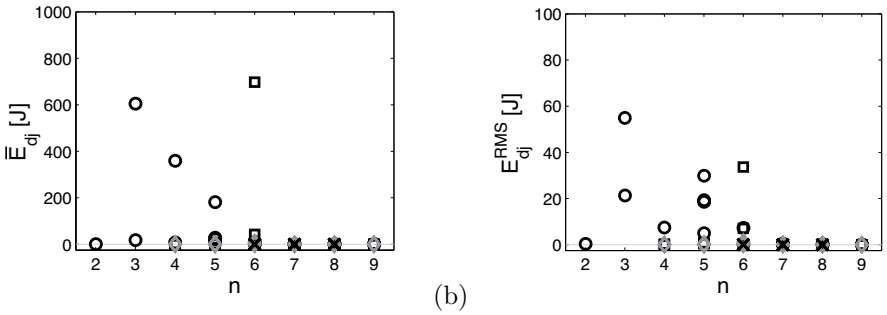

(a) (b)

Figure 7: (a) Mean and (b) RMS of modal deformation energy $E_{\mathrm{d}j}(t)$ of the structural response of the single silo in the two-way coupled simulation. The deformation energy for the lowest 50 eigenmodes is plotted as a function of n while separate mode shapes $(1, n)$ are depicted as a circle ($\circ$), $(2, n)$ as a square ($\square$), $(3, n)$ as a diamond ($\Diamond$), and $(4, n)$ as a cross ($\times$).

By comparison of the one-way and two-way coupled simulation results in figures 6 and 7, respectively, differences in absolute terms are less important because of the short simulated time intervals in the two-way coupled simulations. However, while the excited eigenmodes still correspond to the lowest eigenfrequencies, static and RMS values are overall larger in the two-way coupled simulation. Because the structural flexibility is now taken into account, the wake flow is not only influenced by the random incoming wind flow but also by slightly modified separation and wake behaviour that in turn influence the aerodynamic pressures. The simulated time frame is too short to clarify the difference between the one-way and two-way simulations. It can therefore not decisively be concluded whether the ovalling vibrations of the single silo are related to forced resonance or aeroelastic effects.

4 SILO GROUP SIMULATIONS

The influence of the location of a silo in the group arrangement is investigated by performing one-way coupled simulations for the silo at the windward corner of the group and for the silo at the leeward side of the group (figure 1b).

First, the structural response of silo at the windward corner of the silo group is calculated. The mean and RMS values of the modal deformation energy are shown in figure 8. It can be observed that the static deformation (figure 8a) as well as the vibrations (figure 8b) of this silo are dominated by eigenmodes $(1, 3)$ and $(1, 4)$. Other mode shapes with low circumferential wavenumbers are also excited, but less pronounced. The largest structural displacements are found in the small gaps between two adjacent silos as a result of the larger wind velocities and negative surface pressures in these narrow passages. The magnitude of the structural displacements is as high as 7 cm at these locations which is large compared to the total distance of 30 cm between two neighbouring silos. Vibration

amplitudes are again much smaller than the static deformation (approx. 1 to 2 cm). At the same time, the RMS values for this silo in the group arrangement are larger than for the single isolated silo, indicating larger structural vibrations.

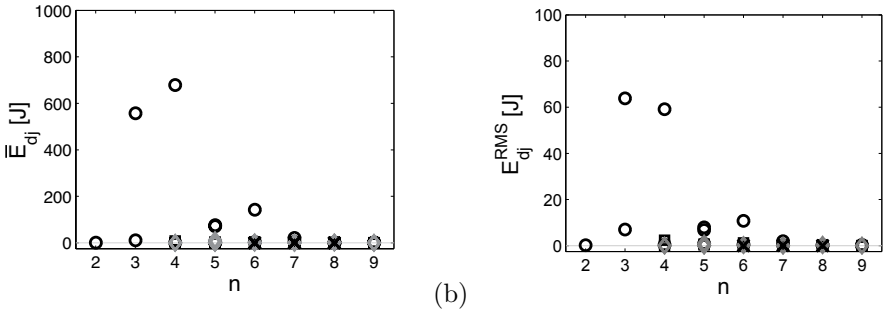

(a) (b)

Figure 8: (a) Mean and (b) RMS of modal deformation energy $E_{\mathrm{d}j}(t)$ of the structural response of the windward corner silo in the one-way coupled simulation of the silo group. The deformation energy for the lowest 50 eigenmodes is plotted as a function of n while separate mode shapes $(1, n)$ are depicted as a circle ($\circ$), $(2, n)$ as a square ($\square$), $(3, n)$ as a diamond ($\Diamond$), and $(4, n)$ as a cross ($\times$).

The results of the one-way coupled simulation for the leeward corner silo of the 8 by 5 silogroup are shown in figure 9. As opposed to silos at the windward side of the silogroup, the modal deformation energy for this silo is negligibly small for all eigenmodes. The radial static displacements are only approx. 1 cm and vibration amplitudes are negligibly small for the leeward corner silo.

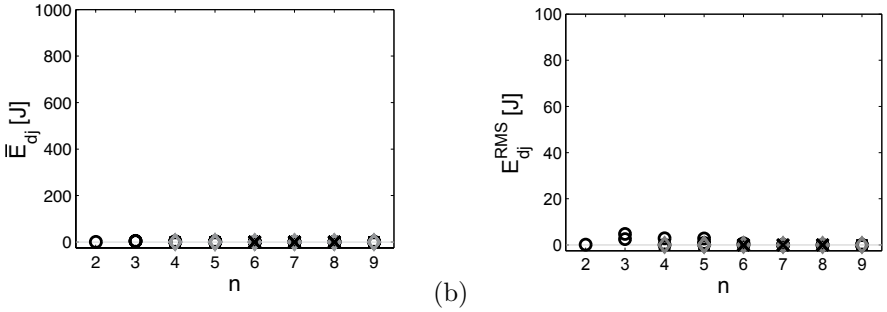

(a) (b)

Figure 9: (a) Mean and (b) RMS of modal deformation energy $E_{\mathrm{d}j}(t)$ of the structural response of the leeward corner silo in the one-way coupled simulation of the silo group. The deformation energy for the lowest 50 eigenmodes is plotted as a function of n while separate mode shapes $(1, n)$ are depicted as a circle ($\circ$), $(2, n)$ as a square ($\square$), $(3, n)$ as a diamond ($\Diamond$), and $(4, n)$ as a cross ($\times$).

The predicted vibration patterns correspond well with the observed ovalling vibrations in the Antwerp silo group. The largest vibrations are observed at the windward side of the group and the mode shapes that are preferentially excited seem to correspond with observations. Vibration levels are still smaller than the ones observed in October 2002.

This may be due to simplifications in the numerical model but is possibly also related to aeroelastic effects.

In the silo group arrangement, the vicinity of the neighbouring silos may have a significant impact on the structural vibrations. Considering the peak structural displacements up to approx. 8 cm at the windward side of the group with respect to the limited distance of 30 cm between two adjacent rigid silos, very different and possibly aeroelastic effects should be considered in a fully coupled FSI simulation.

The location of these large peak displacements has important implications for the numerical solution of the coupled WSI problem, however. A direct transfer of the large structural displacements inevitably leads to a change in the fluid solver that causes a long and large transition in the structural response. Apart from the fact that the spring smoothing ALE mesh update in the fluid solver cannot handle such large mesh deformations, the amplitudes of structural vibration during this transition are so large in the narrow gaps between two silos, that neighbouring silos collide. The ALE mesh update then obviously fails and it is difficult to calculate the two-way coupled simulation.

To reduce the transitional effects as much as possible, a solution is proposed to gradually increase the pressures that are applied in the structural solver during a limited period of time at the start of the two-way coupled simulation. Furthermore, the Laplacian smoothing method is applied to handle the more challenging ALE mesh updates in the narrow gaps between adjacent silos in the fluid solver. This results in a significant increase of the overall simulation time. Simulating 1 s of wind flow in this two-way coupled simulation of one flexible silo in the silo group, requires about 70 hours of computing time on 16 parallel cores and no results have been obtained for this configuration yet.

5 CONCLUSIONS

It is investigated if observed wind-induced ovalling vibrations in a silo group can be predicted by means of numerical simulations. More specifically, the necessity of performing computationally demanding wind-structure interaction (WSI) simulations is assessed. For this purpose, both one-way and two-way coupled simulations are performed.

Before considering the entire silo group, one-way and two-way coupled simulations of a single silo in crosswind are performed. For this configuration, it cannot decisively be concluded if the ovalling vibrations are due to forced resonance or aeroelastic effects because the simulated time frames are too short.

The results of the one-way coupled simulations for the silo group are in reasonably good agreement with observations. Although vibration amplitudes are significantly smaller, it is found that the structural modes with the lowest natural frequencies are excited at the windward side of the silo group. WSI simulations seem to be required however for a correct prediction of the observed vibration amplitudes. As a result of the geometry of the silo group, aeroelastic effects may enforce vibrations in the group arrangement but no definitive conclusions are obtained yet due to several numerical issues in the WSI simulation of the silo group.

REFERENCES

[1] Fluent 14.5. *User's Guide*. Ansys Inc., 2012.

[2] Abaqus 6.10. *User's Manual*. Dassault Systèmes Simulia Corp., 2010.

[3] J. Degroote, K.-J. Bathe, and J. Vierendeels. Performance of a new partitioned procedure versus a monolithic procedure in fluid-structure interaction. *Computers and Structures* (2009) **87**:793–801.

[4] D. Dooms, G. Degrande, G. De Roeck, and E. Reynders. Finite element modelling of a silo based on experimental modal analysis. *Engineering Structures* (2006) **28**(4):532–542.

[5] F.R. Menter and M. Kuntz. Adaptation of eddy-viscosity turbulence models to unsteady separated flow behind vehicles. In R. McCallen, R. Browand, and J. Ross, editors, *Symposium on the aerodynamics of heavey trucks, buses and trains*, Monterey, USA, December 2002. Springer, Berlin Heidelberg New York, 2004.

[6] M.P. Païdoussis, S.J. Price, and E. de Langre. *Fluid-Structure Interactions: Cross-Flow-Induced Instabilities*. Cambridge University Press, Cambridge, 2011.

[7] M.P. Païdoussis, S.J. Price, and H.C. Suen. Ovalling Oscillations of Cantilevered and Clamped-Clamped Cylindrical Shells in Cross Flow: An Experimental Study. *Journal of Sound and Vibration* (1982) **83**(4):533–553.

[8] A. Smirnov, S. Shi, and I. Celik. Random Flow Generation Technique for Large Eddy Simulations and Particle-Dynamics Modeling. *Journal of Fluids Engineering, Transactions of the ASME* (2001) **123**:359–371.

[9] P.R. Spalart, W.-H. Jou, M. Strelets, and S.R. Allmaras. Comments on the feasibility of LES for wings, and on a hybrid RANS/LES approach. In *Proceedings of first AFOSR international conference on DNS/LES*, Ruston, Louisiana, August 1997. Greyden Press.

[10] Y. Tominaga, A. Mochida, R. Yoshie, H. Kataoka, T. Nozu, M Yoshikawa, and T. Shirisawa. AIJ guidelines for practical applications of CFD to pedestrian wind environment around buildings. *Journal of Wind Engineering and Industrial Aerodynamics* (2008) **96**:1749–1761.